Mon. Not. R. astr. Soc. (1986) **221,** 339–364

The stability of accretion tori – I. Long-wavelength modes of slender tori

Peter Goldreich, Jeremy Goodman★ and Ramesh Narayan† *Theoretical Astrophysics, California Institute of Technology, Pasadena, CA 91125, USA*

Accepted 1986 February 5. Received 1986 February 5; in original form 1985 November 11

Summary. We elucidate the inviscid instabilities of an isentropic torus found previously by Papaloizou & Pringle. The torus is a polytrope of index, n, and has a small ratio of minor radius, a, to orbital radius, r_0. In equilibrium it rotates on cylinders with angular velocity profile $\Omega \propto r^{-q}$. Linear modes are proportional to $\exp i(m\phi - \omega t)$. For small $\beta \equiv ma/r_0$, we justify the use of height-averaged equations by appealing to approximate vertical hydrostatic equilibrium. The effective polytropic index for the resulting two-dimensional problem is $N \equiv n + \frac{1}{2}$; thus an incompressible torus in three dimensions behaves compressibly in two. Height-averaged modes obey an ordinary differential equation, which we solve numerically to obtain the growth rate as a function of q, n, and β. The error made in predicting the growth rate of the actual three-dimensional system is small everywhere along the principal branch even for $\beta \sim 0.5$, and is less than 1 per cent for the fastest-growing mode. We analytically solve the artificial case $n = -\frac{1}{2}$, which is two-dimensionally incompressible, and show that it has all the qualitative features of the general case, except that it does not have a resonance at corotation. In the general case, with $n > -\frac{1}{2}$ and $q < 2$, the corotation resonance absorbs energy and angular momentum, so the growing and decaying modes do not occur in complex–conjugate pairs. We solve a second special case, namely $n = 2 - q = 0$, almost analytically in three dimensions, without height-averaging. Papaloizou & Pringle asserted that this system is stable but we show that there is an unstable mode for small β just as in the other systems. In fact this principal unstable branch, with corotation at the pressure maximum, is qualitatively the same for all n and is essentially independent both of compressibility and of the gradient in vorticity per unit surface density. Thus the modes are not sonic, nor are they similar to those of the Kelvin–Helmholtz instability. Instead they are composed of two edge waves, akin to surface waves in water although modified by shear and rotation, coupled across a forbidden region around corotation.

★ Present address: School of Natural Sciences, Institute for Advanced Study, Princeton, NJ 08540, USA.
† Present address: Department of Astronomy, University of Arizona, Tucson, AZ 85721, USA.

1 Introduction

At high mass-accretion rates and at luminosities comparable to the Eddington limit, radiation pressure causes the inner parts of an accretion disc to thicken into roughly toroidal shape; because the geometry is not spherical, even super-Eddington luminosities are possible, and most of the radiation emerges from a narrow empty region, or 'funnel', around the rotation axis (Shakura & Sunyaev 1973; Fishbone & Moncrief 1976; Paczyński & Wiita 1980; Jaroszyński, Abramowicz & Paczyński 1980). Such funnels may expel a wind (Shakura & Sunyaev 1973) and have been proposed as sites for the acceleration and collimation of jets observed in extragalactic radio sources (Lynden-Bell 1978). It has also been proposed that at lower acretion rates and low optical depth, an accretion torus may be supported by the thermal pressure of ions if their cooling time is longer than an orbital period, but shorter than the electron–ion equipartition time (e.g. Rees 1980). Magnetic fields anchored to such tori may extract rotational energy from an accreting black hole and power a radio jet with high mechanical efficiency (Blandford & Znajek 1977; Rees *et al.* 1982). Observational evidence has been claimed for the existence of an accretion torus in SS433 (Margon 1984 and references therein).

The recent discovery by Papaloizou & Pringle (1984, 1985 – henceforth PPI and PPII) that accretion tori can be dynamically unstable is of great importance in astrophysics because of the possibility that they form part of the central engine in active galactic nuclei and quasars [*cf.* Rees (1984) and Begelman, Blandford & Rees (1984)]. More generally, the instability provides an instructive example of global, non-axisymmetric instability in a differentially rotating system, and some of the lessons learned from its study will apply to rotating stars, planetary rings, and disc galaxies. Among these astronomical systems, the accretion disc or torus is perhaps the simplest because self-gravity can normally be neglected (but see Kozłowski, Wiita & Paczyński 1979). Magnetic effects and radiative viscosity may not be negligible in general but we neglect them here. Strictly speaking, we neglect the accretion process itself, since we perturb about an exactly stationary state of an ideal, isentropic fluid rotating on cylinders with angular-velocity profile $\Omega \propto r^{-q}$. We also neglect relativistic effects. The details of the equilibrium are discussed in PPI.

Pressure gradients cause the rotation law to depart from Keplerian ($q=3/2$). If the gradients are so large that $q>2$, then the specific angular momentum decreases outwards, and the torus is *locally* and *axisymmetrically* unstable (Rayleigh 1880, 1916). PPI showed that the marginal case, $q=2$, suffers *non-axisymmetric*, *global instabilities*. Blaes (1985) obtained analytic estimates of the growth rate in the limit of small $\beta \equiv ma/r_0$ for $q=2$ and arbitrary polytropic index, n; here m is the azimuthal mode number, a is the minor radius of the torus, and r_0 is the orbital radius of the pressure maximum.★ PPII argued that tori are unstable throughout the range $\sqrt{3}<q<2$ for $n>0$, but they attributed the instabilities to a mixture of two physical mechanisms; a sonic instability that predominates near $q=2$, and a Kelvin–Helmholtz-like instability that requires a maximum in the vorticity per unit surface density and dominates near $q=\sqrt{3}$.

In this paper we restrict ourselves to what we refer to as the principal or long-wavelength branch of the dispersion relation of a slender torus. It is the only branch which may be unstable in the limit of infinite azimuthal wavelength. Higher order branches were considered first in PPI and PPII and subsequently by Goldreich & Narayan (1985). We will return to these more slowly growing modes in a later paper.

We offer three main contributions to the understanding of Papaloizou & Pringle's long-wavelength instabilities. The first is to provide quantitative estimates of the growth rate as a function of q, n and β. Earlier work has been restricted to one or more of the special limits $q\to 2$, $q\to\sqrt{3}$, or $\beta\to 0$. To this end, we develop and justify in Section 2 the use of height-averaged fluid equations. The governing equation for linear modes is thereby reduced from a partial to an

★ Blaes used the symbol β to denote a quantity that reduces to a/r_0 for $a \ll r_0$.

ordinary differential equation, and in Section 3 we derive growth rates for the height-averaged system. In the Appendix departures from vertical hydrostatic equilibrium are treated as a perturbation, and we show thereby that the estimates of Section 3 are accurate to better than 1 per cent at maximum growth.

Our second contribution is to identify correctly the physical mechanism underlying these instabilities. In Section 4 we solve exactly for the two-dimensional modes when $n=-1/2$. Although the three-dimensional torus for this n is rather peculiar, the height-averaged system corresponds to incompressible, two-dimensional flow which is shown in Section 3 to behave similarly to tori with $n\geq 0$. The true origin of Papaloizou & Pringle's instability emerges in Section 4 from a detailed examination of this special case. Our interpretation differs from that of PPII, for we find that it is neither compressibility nor the maximum in vorticity per unit surface density which drives the torus to instability. Instead the modes are most naturally interpreted as edge waves propagating backwards at the inner edge of the torus and forwards at the outer edge, coupled to each other across corotation, which is located at the pressure maximum. For a two-dimensionally incompressible fluid, the edge mode has an obvious physical meaning since it is the only possible disturbance. In compressible tori, edge modes propagate along the natural soft edge provided by the density gradient. They are akin to the f-modes of polytropic stars.

Our third contribution is to identify the role of the corotation resonance. Its presence is reflected by a singularity in the differential equation of the height-integrated system whenever there is a non-zero gradient of vorticity per unit surface density (which requires $q<2$ and $n>-1/2$). When the singularity is handled according to the standard prescription to satisfy causality, the symmetry between the growing and decaying modes is broken. In particular, there are regions of parameter space where both principal modes decay.

We treat the special case $q=2$, $n=0$ at length in Section 5 for several reasons. First, the modes can be found easily in this case without height-averaging, and therefore we have a further check on that approximation. Secondly, PPI asserted that this system is stable, whereas we show by construction in Section 5 that it is not. Thirdly, higher-frequency branches of instability emerge which are not well described by height-averaging. We intend to show in a second paper that these higher branches extend to $q<\sqrt{3}$, although their growth rates diminish rapidly as $q\rightarrow 3/2$. Finally, Section 6 contains a summary and discussion of results.

2 Linear perturbations of a narrow torus

2.1 THE EQUILIBRIUM SYSTEM

We consider a narrow torus lying between radii (r_0-a) and (r_0+a) with $a\ll r_0$. We take the angular velocity profile to have the form:

$$\Omega(r)=\Omega\left(\frac{r_0}{r}\right)^q, \qquad \Omega=\text{constant}. \tag{2.1}$$

We will be interested in the range of q between 3/2, corresponding to a Kepler disc, and 2, corresponding to a constant angular momentum torus. We adopt a polytropic equation of state, so that the pressure, p, and density, ϱ, are related by

$$p=K\varrho^{\Gamma}\equiv K\varrho^{1+1/n}. \tag{2.2}$$

The polytropic index n measures the three-dimensional compressibility, $n=0$ and $n=\infty$ correspond to incompressible and isothermal fluids, respectively.

Since the torus is narrow it is convenient to introduce quasi-Cartesian coordinates with $x=(r-r_0)$ taken along the radial direction, $y=r_0\phi$ along the tangential direction, and z perpen-

dicular to the equatorial plane. In this approximation, the equilibrium flow viewed in a frame rotating with angular velocity $\Omega(r_0)$ is given by;

$$\mathbf{V}=2Ax\hat{j}, \tag{2.3}$$

$$2A\equiv -q\Omega, \tag{2.4}$$

where $\hat{i}$, $\hat{j}$, $\hat{k}$ are unit vectors along the Cartesian axes. The vorticity in the flow is

$$\nabla\times\mathbf{V}=2B\hat{k}, \tag{2.5}$$

$$B\equiv A+\Omega=\frac{(2-q)\Omega}{2}. \tag{2.6}$$

We neglect the variation of Ω, A, and B within the torus. The relative gravitational acceleration is taken to be positive towards the interior of the torus. Its value at the point (x, y, z) due to the central point mass around which the torus orbits is

$$-\mathbf{g}_G=3\Omega^2x\hat{i}-\Omega^2z\hat{k}, \tag{2.7}$$

whereas the Coriolis acceleration is

$$-\mathbf{g}_C=-2\Omega\hat{k}\times\mathbf{V}=-2q\Omega^2x\hat{i}. \tag{2.8}$$

The effective gravity is thus,

$$\mathbf{g}_{\rm eff}\equiv\mathbf{g}_C+\mathbf{g}_G=(2q-3)\Omega^2x\hat{i}+\Omega^2z\hat{k}. \tag{2.9}$$

The net acceleration towards the torus interior is balanced by the pressure gradient.

The equilibrium structure of the torus is worked out in PPI. The density, pressure, and enthalpy, $Q_0=(n+1)p/\varrho$, are given by

$$\varrho(x, z)=\left[\frac{\Omega^2}{2(n+1)K}\right]^n[h^2(x)-z^2]^n, \tag{2.10}$$

$$p(x, z)=K\left[\frac{\Omega^2}{2(n+1)K}\right]^{(n+1)}[h^2(x)-z^2]^{(n+1)}, \tag{2.11}$$

$$Q_0(x, z)=(1/2)\Omega^2[h^2(x)-z^2], \tag{2.12}$$

where

$$h^2(x)=(2q-3)(a^2-x^2). \tag{2.13}$$

The minor cross-section of the torus is thus an ellipse with radial diameter $2a$ and vertical diameter $2(2q-3)^{1/2}a$.

2.2 LINEARIZED PERTURBATION THEORY

Let the Eulerian velocity perturbation be u, v, and w along the three Cartesian axes, and let the pressure, density, and enthalpy perturbations be p', ϱ', and Q. Since the equilibrium system is invariant with respect to y and t, we can without loss of generality take the perturbations to have the form

$$u(x, y, z, t)=u(x, z)\exp[i(ky-\omega t)], \text{ etc.} \tag{2.14}$$

In terms of the original torus problem

$$k=m/r_0, \tag{2.15}$$

where m is the azimuthal mode number of the disturbance. In this paper, we are interested in modes with azimuthal wavelength, $2\pi/k$, large compared to a. Hence, we define the small parameter

$$\beta=ka\ll 1. \tag{2.16}$$

In fact, we later allow values of $\beta\sim 1$. Although β can only take a discrete set of values [see equation (2.15)], we find it convenient to think of β as a continuous variable. We write ω in terms of a reduced frequency, s,

$$\omega=2A\beta s=-q\Omega\beta s, \tag{2.17}$$

and define $\sigma(x)$ to be the Doppler-shifted frequency of the pattern as seen by the unperturbed fluid at x,

$$\sigma(x)=\omega-2Akx=-2A\beta\left(\frac{x}{a}-s\right)=q\Omega\beta\left(\frac{x}{a}-s\right). \tag{2.18}$$

In the case of unstable modes, s becomes a complex number. Since A is negative, growing modes have $Im(s)<0$, and decaying modes have $Im(s)>0$.

The linearized Euler equations of motion along x and y give

$$-i\sigma u-2\Omega v=-\partial Q/\partial x, \tag{2.19}$$

$$2Bu-i\sigma v=-ikQ. \tag{2.20}$$

These are solved to yield

$$u=\frac{i\sigma}{D}\frac{\partial Q}{\partial x}-\frac{2i\Omega k}{D}Q, \tag{2.21}$$

$$v=\frac{2B}{D}\frac{\partial Q}{\partial x}-\frac{\sigma k}{D}Q, \tag{2.22}$$

$$D=\varkappa^2-\sigma^2, \tag{2.23}$$

where the epicyclic frequency $\varkappa$ is

$$\varkappa=\sqrt{\Omega B}=\sqrt{2(2-q)}\Omega. \tag{2.24}$$

The vertical equation of motion gives

$$-i\sigma w=-\frac{\partial Q}{\partial z}. \tag{2.25}$$

We write the continuity equation with the aid of the equation of state, $\varrho'=(\varrho^2/\Gamma p)Q$, as

$$-i\sigma\frac{\varrho^2}{\Gamma p}Q+ik\varrho v+\frac{\partial}{\partial x}(\varrho u)+\frac{\partial}{\partial z}(\varrho w)=0. \tag{2.26}$$

Then, eliminating the velocity components by using equations (2.21), (2.22), and (2.25), we obtain the following partial differential equation for Q

$$\left[\frac{\sigma^2\varrho^2}{\Gamma p}+\frac{\sigma^2k^2\varrho}{D}+2\sigma\Omega k\frac{\partial}{\partial x}\left(\frac{\varrho}{D}\right)\right]Q-\sigma^2\frac{\partial}{\partial x}\left(\frac{\varrho}{D}\right)\frac{\partial Q}{\partial x}-\frac{\sigma^2\varrho}{D}\frac{\partial^2Q}{\partial x^2}+\frac{\partial}{\partial z}\left(\varrho\frac{\partial Q}{\partial z}\right)=0. \tag{2.27}$$

This is very similar to equation (2.19) for $W=Q/\sigma$ derived in PPII. The few small differences can be traced to our neglect of the azimuthal curvature of the torus through our Cartesian approxima-

tion. These terms are not important and so we expect equation (2.27) to capture all the essential physics of the narrow torus.

The boundary condition at the surface is that the Lagrangian pressure perturbation vanishes. Thus, we require

$$p'+\boldsymbol{\xi}\cdot\nabla p=0 \tag{2.28}$$

where $\boldsymbol{\xi}$ is the displacement at the surface. To first order, $-i\sigma\boldsymbol{\xi}=\mathbf{v}'+(\boldsymbol{\xi}\cdot\nabla)\mathbf{V}$, where $\mathbf{v}$ is the Eulerian velocity perturbation, and in the equilibrium $\nabla p=-\varrho\mathbf{g}_{\rm eff}$. Using these relations and equations (2.9), (2.21), and (2.25), we can rewrite (2.28) in terms of Q:

$$\frac{(2q-3)\Omega^2\sigma^2}{D}x\frac{\partial Q}{\partial x}-\Omega^2 z\frac{\partial Q}{\partial z}=\left[\frac{2(2q-3)\Omega^3\sigma kx}{D}-\sigma^2\right]Q. \tag{2.29}$$

Note that this boundary condition is required if Q is to be a regular solution of equation (2.27) as $\varrho\to 0$.

2.3 VERTICAL HYDROSTATIC EQUILIBRIUM

Several pieces of evidence suggest that the low-β modes which we consider in this paper involve essentially two-dimensional motions in the horizontal plane. First, we have developed an exact analysis of the incompressible ($n=0$) constant angular momentum ($q=2$) torus. The three-dimensional solutions for this special case are discussed in Section 5. As shown by Fig. 5(b, c), the contours of the enthalpy Q are nearly vertical. This means Q is almost independent of z and thus by equations (2.21) and (2.22), that u and v are also independent of z. Secondly, we develop in the Appendix a perturbation theory to estimate the magnitude of the correction to the growth rate of unstable modes due to z-dependent motions. As shown there, the corrections are remarkably small throughout the range of interest, even though this extends to $\beta\sim 1$. We present here a third argument in favour of two-dimensional motions by showing that vertical accelerations are negligible at small β so that the torus is always in nearly perfect vertical hydrostatic equilibrium.

Let us *assume* that vertical hydrostatic equilibrium is satisfied at all times, and try to estimate the error we make from this assumption. At each instant, the structure of the torus is given by equations (2.10)–(2.12) except that $h(x)$ is modified because of the two-dimensional velocity divergence which causes the height of each vertical column of fluid to oscillate at frequency σ. The resulting non-hydrostatic vertical acceleration is smaller than the gravitational acceleration by order $(\sigma/\Omega)^2$. Thus we expect the non-hydrostatic correction to the enthalpy perturbation to be of this order relative to the dominant hydrostatic contribution.

A more rigorous estimate of the non-hydrostatic part of the perturbed enthalpy is obtained as follows. Let $h'(x)$ be the perturbation in $h(x)$. From equation (2.12) we then see that the perturbed enthalpy is

$$Q_{\rm HS}=\Omega^2 hh', \tag{2.30}$$

where, in this subsection and the Appendix only, we use the subscript HS, to serve as a reminder of the hydrostatic approximation. Since $Q_{\rm HS}$ in independent of z, so too are u and v as argued above. The part of the motion that is ignored in the hydrostatic assumption is the vertical velocity w. Let us now estimate the enthalpy perturbation due to this. Since h' oscillates with frequency σ, the perturbed vertical velocity at the surface is $-i\sigma h'+udh/dx$, and the velocity as a function of z is

$$w=-i\sigma h'\frac{z}{h}+u\frac{dh}{dx}\frac{z}{h}. \tag{2.31}$$

Substituting this into equation (2.25) and using equations (2.21) and (2.30), we find the perturbation in the enthalpy due to vertical accelerations, Q', to be given by

$$Q'(x, z)=\Delta Q(x)+\delta Q(x, z), \tag{2.32}$$

where

$$\delta Q(x, z)=\frac{\sigma^2}{2D}\left\{x\frac{dQ_{\rm HS}}{dx}+\left[\frac{D}{(2q-3)\Omega^2}-\frac{2\Omega kx}{\sigma}\right]Q_{\rm HS}\right\}\left(\frac{z}{a}\right)^2. \tag{2.33}$$

We note that δQ vanishes at $x=\pm a$ as a consequence of the boundary condition (2.29) applied to $Q_{\rm HS}$. For $\beta^2\ll 1$, we expect δQ to vary slowly with x and thus remain small compared to $Q_{\rm HS}$ everywhere within the torus. Furthermore, for $q<2$, $\sigma^2/D\to 0$ as $\beta\to 0$, which provides additional support for the z-independence of the long-wavelength modes. To complete the justification of the hydrostatic assumption, we must show that ΔQ is small compared to $Q_{\rm HS}$ for $\beta\ll 1$. That this is true follows from the Appendix. Equation (A10) reveals that $\delta Q\to 0$ implies $\Delta s\to 0$ which in turn implies, from equation (A8), that $\Delta Q\to 0$. Thus the hydrostatic approximation becomes exact as $\beta\to 0$.

From equation (2.10), we obtain the height-integrated surface density $\Sigma(x)$ to be

$$\Sigma(x)=\int_{-h(x)}^{h(x)}\varrho(x, z)dz=\Sigma_0\left(1-\frac{x^2}{a^2}\right)^{n+1/2}. \tag{2.34}$$

Comparing this to equation (2.10), we see that, considered in a two-dimensional sense, the fluid behaves as if it had a polytropic index

$$N=n+1/2. \tag{2.35}$$

This relation applies in both equilibrium and for perturbations. An immediate consequence is that, for hydrostatic low-β modes, the three-dimensionally incompressible torus ($n=0$) is compressible in two dimensions ($N=1/2$) and is thus qualitatively similar to tori with non-zero n. The special system with $N=0$ i.e. $n=-1/2$, is two-dimensionally incompressible. This system, which we call the thin ribbon, is discussed in some detail in Section 4.

2.4 HEIGHT-INTEGRATED EQUATIONS

Armed with the knowledge that Q, u, and v are essentially independent of z, we now derive simplified equations for the two-dimensional motion. We integrate the continuity equation (2.26) with respect to z, using equations (2.10), (2.11), and (2.34) to obtain

$$-\frac{i(2n+1)\sigma}{(2q-3)\Omega^2(a^2-x^2)}Q+ikv+\frac{d\ln\Sigma}{dx}u+\frac{du}{dx}=0. \tag{2.36}$$

Substituting for u and v from (2.21) and (2.22), we obtain an ordinary differential equation for Q:

$$\frac{d^2Q}{dx^2}+\frac{d\ln(\Sigma/D)}{dx}\frac{dQ}{dx}-\left[\frac{2\Omega k}{\sigma}\frac{d\ln(\Sigma/D)}{dx}+\frac{(2n+1)D}{(2q-3)\Omega^2(a^2-x^2)}+k^2\right]Q=0. \tag{2.37}$$

Inserting the appropriate expressions for Σ and D, this takes the form

$$\frac{d^2Q}{d\xi^2}-\left[\frac{(2n+1)\xi}{(1-\xi^2)}-\frac{2q^2\beta^2(\xi-s)}{2(2-q)-q^2\beta^2(\xi-s)^2}\right]\frac{dQ}{d\xi}$$
$$-\left\{\frac{(2n+1)[2(2-q)-q^2\beta^2(\xi-s)^2]}{(2q-3)(1-\xi^2)}-\frac{2(2n+1)\xi}{q(\xi-s)(1-\xi^2)}+\frac{4q\beta^2}{2(2-q)-q^2\beta^2(\xi-s)^2}+\beta^2\right\}Q=0, \tag{2.38}$$

where we have defined the normalized independent variable

$$\xi=\frac{x}{a}. \tag{2.39}$$

We employ the free boundary condition at $\xi=\pm 1$. Thus, setting the Lagrangian pressure perturbation at the two ends to zero, we require $Q+(iu/\sigma\varrho)(dp/dx)=0$, which translates to

$$\frac{(2q-3)\Omega^2\xi}{D}\frac{dQ}{d\xi}=\left[\frac{2(2q-3)\Omega^3\beta\xi}{\sigma D}-1\right]Q. \tag{2.40}$$

Of the two independent solutions of equation (2.38), one is well-behaved at the boundaries and the other is singular. The boundary condition (2.40) automatically picks the well-behaved solution.

The differential equation (2.38) appears to have three singularities, one at corotation where $\xi=s$, and one at each of the Lindblad resonances where $D=0$ i.e. $(\xi-s)^2=2(2-q)/q^2\beta^2$. Actually, the Lindblad resonances are only apparent singularities in the Q equation, and in fact cause no complication. This is directly demonstrated by deriving a differential equation for one of the other variables, say u. To do this, we solve equations (2.20) and (2.36) to obtain Q and v in terms of u and du/dx,

$$Q=\frac{i\sigma c^2}{F}\frac{du}{dx}+\frac{ic^2}{F}\left(\sigma\frac{d\ln\Sigma}{dx}+2Bk\right)u, \tag{2.41}$$

$$v=\frac{ikc^2}{F}\frac{du}{dx}+\frac{ic^2}{F}\left(k\frac{d\ln\Sigma}{dx}+\frac{2B\sigma}{c^2}\right)u, \tag{2.42}$$

$$F=c^2k^2-\sigma^2, \tag{2.43}$$

where we have defined the two-dimensional sound speed c,

$$c^2=\frac{(2q-3)\Omega^2}{(2n+1)}(a^2-x^2). \tag{2.44}$$

Substituting for Q and v in equation (2.19), we obtain a second-order differential equation for u,

$$\frac{d^2u}{dx^2}+\frac{d\ln(\Sigma c^2/F)}{dx}\frac{du}{dx}+\left[\frac{2Bk}{\sigma}\frac{d\ln(c^2/\Sigma F)}{dx}+\frac{F}{c^2}\frac{d}{dx}\left(\frac{c^2}{F}\frac{d\ln\Sigma}{dx}\right)-\frac{D}{c^2}-k^2\right]u=0. \tag{2.45}$$

The corotation singularity at the point where $\sigma=0$ still survives. However, there is no sign of the singularities at the Lindblad resonances, $D=0$, which proves that these are not real singularities. Instead, equation (2.45) has a new pair of apparent singularities where $F=c^2k^2-\sigma^2=0$; clearly, these are also spurious singularities. Applying the method of Frobenius, it is not difficult to prove that the points where $D=0$ are regular points of equation (2.38) for Q and the points where $F=0$ are regular points of equation (2.45) for u.

The real singularity at $\xi=s$ arises because the fluid at corotation can absorb energy and angular momentum from the mode. Some care has to be exercised in handling this singularity. The correct prescription in such situations is to integrate the differential equation along a contour in the complex plane that satisfies causality (see, for example, discussions of Landau damping). Briefly, we first imagine that the mode is strongly growing, i.e. $Im(\omega)\gg 0$, and choose a preliminary contour along the real ξ axis; we then allow $Im(\omega)$ to relax to its true value while distorting the contour, if necessary, to prevent the corotation singularity from crossing it (the distortion is necessary only for a neutral or decaying mode). Only with such a contour do we find a mode that is

equivalent to some initial value problem. Because A in equation (2.17) is negative, growing modes have $Im(s)<0$, and, therefore, the contour in complex ξ-space along which we integrate (2.38) is chosen to lie in the upper half-plane, *above* the pole at $\xi=s$. One effect of this is that, although the differential equation and the boundary condition have real coefficients, the eigenvalues, s, still do not occur in complex conjugate pairs. The choice of contour breaks this symmetry. There are two special situations where the corotation resonance has no effect. One is the thin incompressible ribbon ($N=0$ i.e. $n=-1/2$), since the resonant term in equation (2.38) vanishes. The other case is the constant angular momentum torus ($q=2$) where $B=0$ [see equation (2.45)]. In these two cases, eigenvalues occur in complex conjugate pairs.

3 Numerical results

In this section we present numerical results for the growing modes of the height-averaged fluid equations. We will see that, in most respects, the modes are qualitatively independent of the Emden parameter, N.

We regard the dimensionless azimuthal wavenumber $\beta\equiv ka=ma/r_0$ as a continuous variable, and consider first the limit $\beta\to 0$ which corresponds to pretending that the periodicity length in the azimuthal direction is infinitely larger than the minor radius, a. In this limit, the eigenfrequencies ω tend also to zero, and therefore $\sigma=\omega+\beta q\Omega\xi\to 0$; the approximation of vertical hydrostatic equilibrium therefore becomes exact, and so the eigenfrequencies of the height-averaged fluid equations are exactly those of an extremely narrow three-dimensional torus. The limit $\beta\to 0$ has been considered by Blaes (1985) in the special case $q=2$ and by PPII for q near $\sqrt{3}$. The results of this section agree with theirs.

As $\beta\to 0$, equation (2.38) reduces to

$$\frac{d^2Q}{d\xi^2}-\frac{2N\xi}{1-\xi^2}\frac{dQ}{d\xi}-\frac{2N}{1-\xi^2}\left[\frac{2(2-q)}{(2q-3)}-\frac{2\xi}{q(\xi-s)}\right]Q=0, \tag{3.1}$$

and the boundary condition, to

$$\xi\frac{dQ}{d\xi}+\left[\frac{2(2-q)}{(2q-3)}-\frac{2\xi}{q(\xi-s)}\right]Q=0 \qquad \text{at } \xi=\pm 1. \tag{3.2}$$

With the prescription of Section 2 for the integration contour, equations (3.1) and (3.2) have solutions for non-zero, finite s; since $\omega=-q\beta\Omega s$, the eigenfrequencies of these modes tend linearly to zero with β. Fig. 1(a) & (b) show how the real and imaginary parts of $\omega/\beta\Omega=-qs$ depend on q for a few interesting values of $n=N-1/2$. Note that for $q>\sqrt{3}$, growing modes exist with co-rotation at the centre of the torus, i.e. $\xi_c=Re(s)=0$. In the same range of q, a decaying mode also exists but, as discussed in Section 2, in general it does not have the complex–conjugate eigenfrequency.

If $q<\sqrt{3}$, then for $N>0$ there are two decaying modes. At some q between $\sqrt{3}$ and 3/2, the imaginary parts of the two eigenfrequencies merge, and the real parts split into equal and opposite non-zero values. As q decreases further towards 3/2, the co-rotations of the two modes approach opposite edges of the torus, and their common dimensionless growth rate $Im(\omega/\beta\Omega)\to 0$.

It is seen in Fig. 1(b) that the growth rate declines as N increases at fixed β. The decline is caused by the use of a as the characteristic width of the torus. For large N, a more sensible measure is some characteristic width of the surface-density profile, such as $b=a/\sqrt{N+1}$. One can demonstrate that $Im(\omega/kb\Omega)$ has a non-zero limit as $N\to\infty$.

Although its relative simplicity makes it pedagogically interesting, the limit $\beta\to 0$ is of less practical interest than the fastest-growing mode. Fig. 2(a), (b) & (c) are contour maps of the

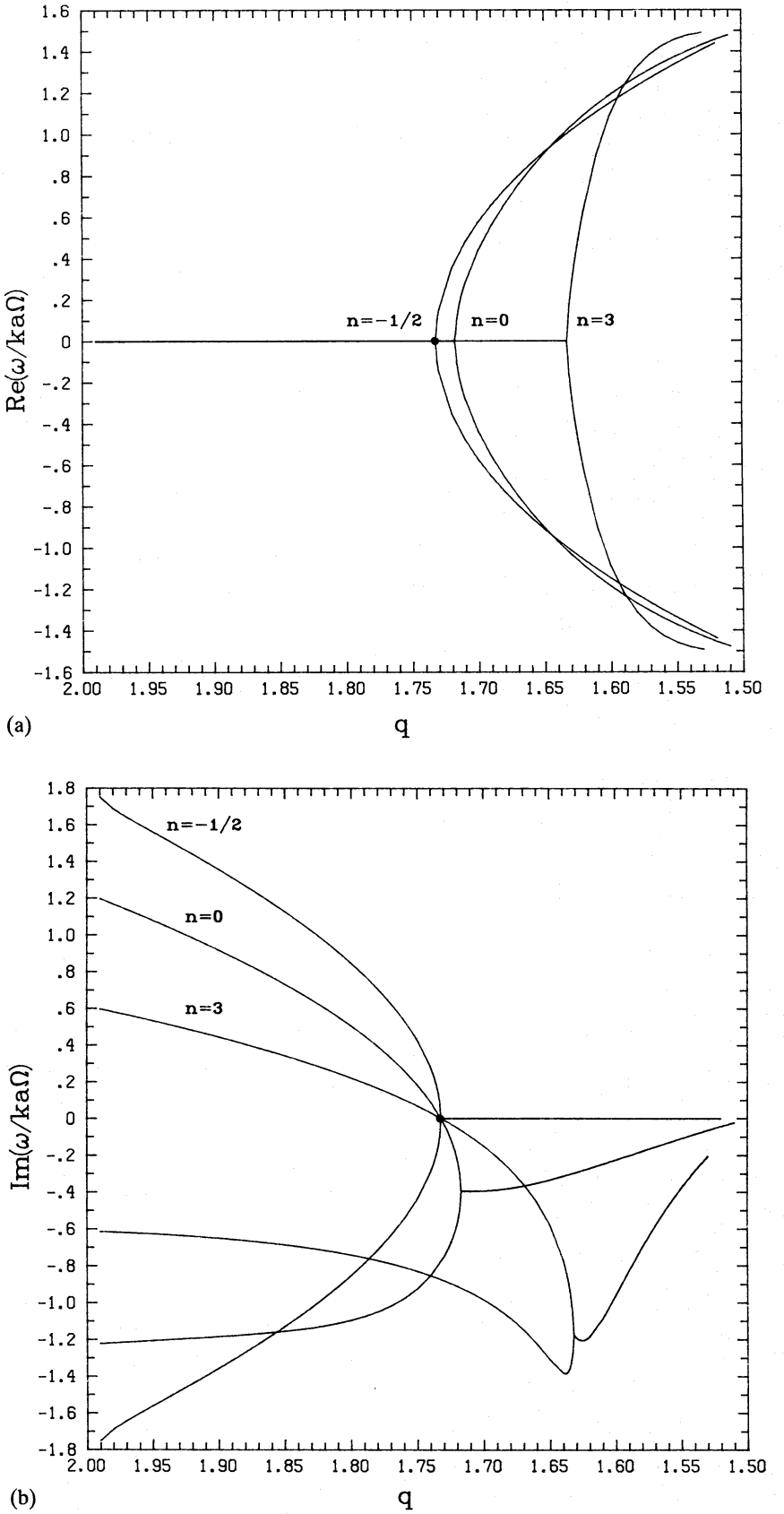

Figure 1. The dimensionless eigenfrequency $\omega/\beta\Omega$ on the principal branch in the limit that the dimensionless wavenumber $\beta \to 0$ for various values of the Emden parameter, n. (a) The real part. Note that all modes shown have corotation within the torus, i.e. $|Re(\omega/\beta\Omega)| < q$. (b) The imaginary part.

physical growth rate $Im(\omega/\Omega)$ of the growing mode as a function of β and q for $N=0, 1/2$, and $7/2$. These maps were computed from the height-averaged equations (2.38)–(2.40), which are *a priori* suspect when β and hence also ω/Ω are not small. The Appendix demonstrates, however, that the error committed by height-averaging is at most 1 per cent throughout the ranges of β, q, and N of

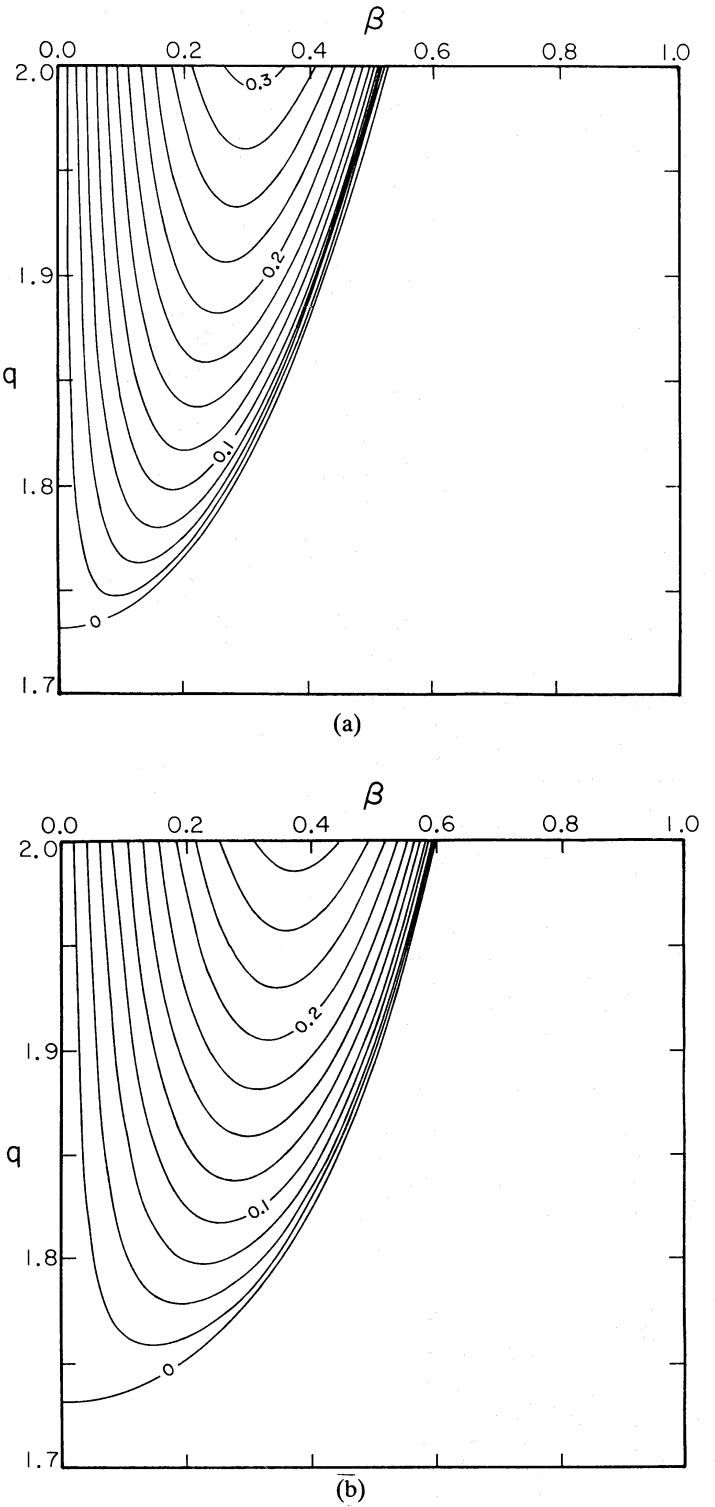

Figure 2. The growth rate in units of the orbital frequency, $Im(\omega/\Omega)$, for (a) $n=-1/2$, (b) $n=0$, and (c) $n=3$. Note that the maximum growth rate is roughly 0.3 for all three cases.

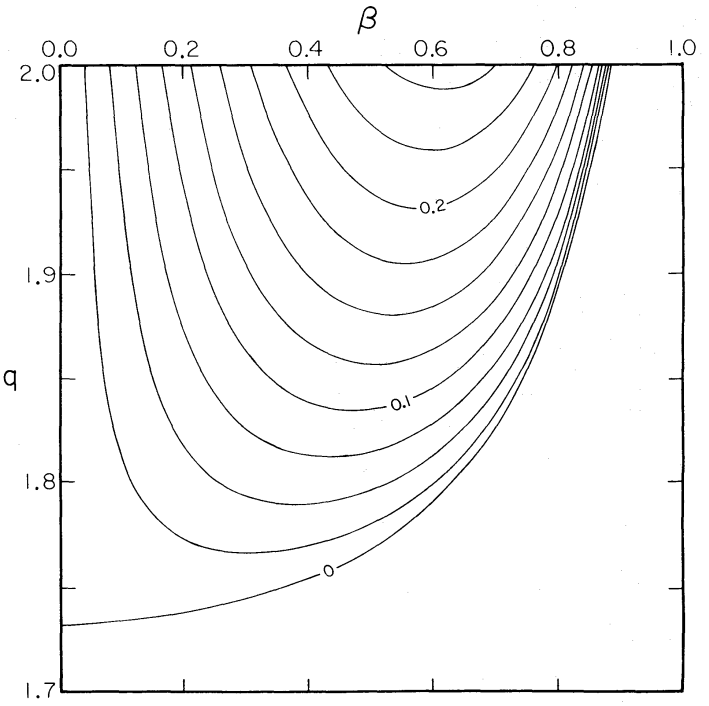

Figure 2 – *continued*

interest. For small β and $q>\sqrt{3}$, the contours are parallel to the q axis. At fixed q, the growth rate rises with increasing β to a maximum at a point β_{max} and then declines again, with a cut-off at $\beta=\beta_c$. Both β_{max} and β_c increase with N; in fact, both are proportional to $\sqrt{N}$ as $N\to\infty$, whereas (in the same notation) $(kb)_{max}$ and $(kb)_c$ are asymptotically constant. Once this rescaling is taken into account, Fig. 2(a), (b) & (c) appear remarkably similar. Even the maximum growth rate is nearly the same: $Im(\omega/\Omega)=0.31$, 0.28, and 0.26 for $N=0$, 1/2, and 7/2 respectively. PPI show that for $n\to\infty$, where the mode is exactly constant with height, $Im(\omega/\Omega)_{max}=0.242$, and this occurs at $(kb)_{max}=0.189$.

Fig. 3(a), (b) & (c) show the perturbed-velocity and perturbed-enthalpy fields for the same three values of N at the wavelength of maximum growth. Again one notices the essential similarity of all three cases, except for the change of radial (x) scale.

The numerical evidence suggests that the same physical mechanism or mechanisms give rise to all of the instabilities in Fig. 3(a), (b) & (c). It is particularly significant that the case $N=0$ does not differ essentially from the rest. This model has neither a gradient in vorticity per unit surface density nor compressibility, and yet it is unstable. Grinfeld (1984) proves, and PPII cite, a theorem that one or both of these effects is necessary for the instability of an inviscid two-dimensional shear flow. However, Grinfeld's theorem is proven under the assumption that u vanishes at the boundaries of the flow. We have used the free boundary condition (2.40) which is the appropriate one for the torus; it is also the only boundary condition permitting a regular solution for the fluid variables near the edge, where $\Sigma\to 0$.

We remark also that, according to the results of this section, the three-dimensionally incompressible, constant-angular-momentum torus ($n=N-1/2=0$, $q=2$) is unstable, contrary to the conclusions given in PPI which rest on an inappropriate choice of boundary conditions. We shall return to this special case in Section 5, where it is shown that the three-dimensional modes of this model can be obtained without height averaging. Those more rigorous results agree very well with the results presented in this section.

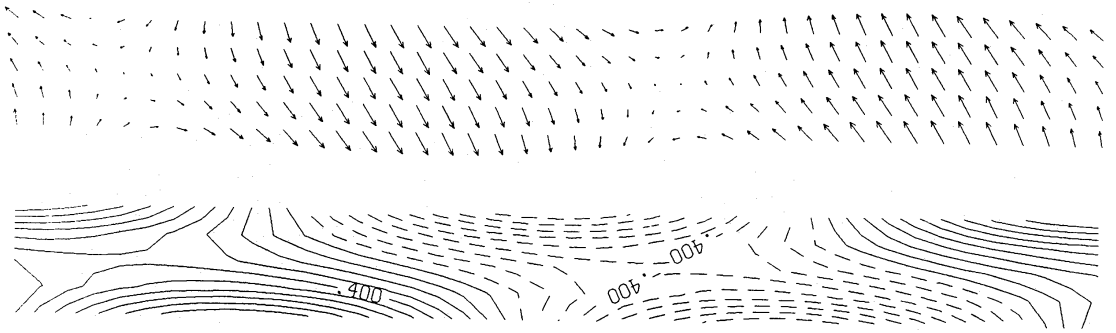

(a)

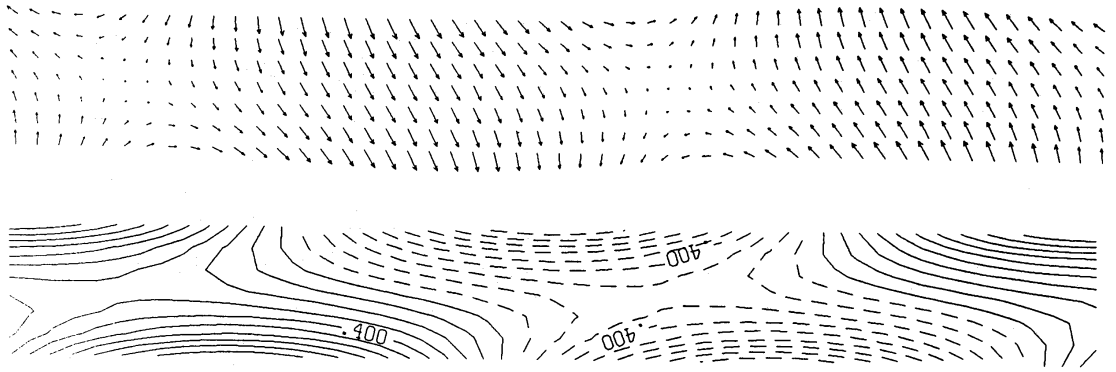

(b)

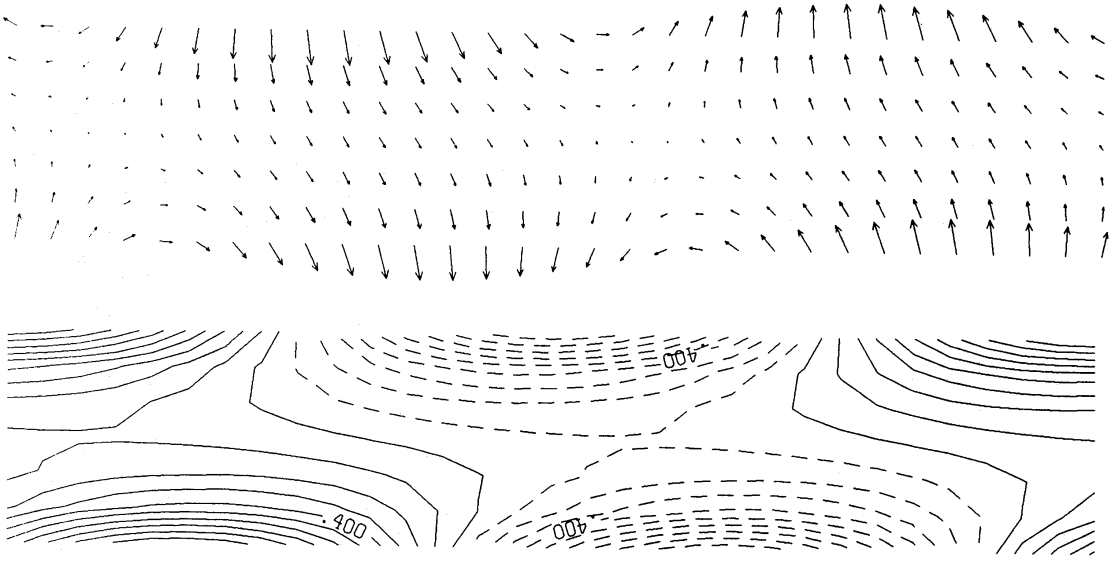

(c)

Figure 3. The height-averaged velocity field (upper) and enthalpy contours (lower) in the orbital plane for the fastest-growing mode on the principal branch for $q=2$. Vertical (x) and horizontal (y) scales are shown in true proportion. Dashed contours mark negative values. (a) $n=-1/2$, (b) $n=0$, (c) $n=3$. The unperturbed angular velocity decreases upward, so the disturbances are leading.

4 The thin ribbon

In Sections 2 and 3 we have alluded to the thin ribbon, the two-dimensionally incompressible limit of the narrow torus. Figs 1–3 establish that the unstable modes of the thin ribbon are qualitatively qualitatively similar to those for the long-wavelength unstable modes of three-dimensional tori. Thus we study this simple model to elucidate the low-β modes of narrow tori.

We follow the notation defined in Section 2 with two notable exceptions. First, we work with dimensionless variables throughout. Thus $\nu \equiv \omega/\Omega$, $\xi \equiv x/a$. The dimensionless σ and $g_{\rm eff}$ are obtained from their dimensional counterparts after division by Ω and $\Omega^2 a$, respectively. Secondly, we augment the effective gravitational acceleration by $p^2\xi$, thus imposing an extra component of inward gravitational acceleration which is not present in the narrow torus. From the obvious dimensionless analogues of equations (2.9) and (2.18), we have

$$\sigma = \nu + q\beta\xi, \tag{4.1}$$

and

$$g_{\rm eff} = g_{\rm G} + g_{\rm C} = (2q + p^2 - 3)\xi. \tag{4.2}$$

The extension to non-zero p is made to aid the interpretation of the unstable modes, as will become clear in Section 4.3. We note that the limit of vanishing rotation, $\Omega \to 0$, corresponds to the limit $q \to \infty$, $p \to \infty$, with p/q=constant.

4.1 DERIVATION OF THE DISPERSION RELATION

The ξ component of the perturbed velocity is the most convenient dependent variable. The linearized equations of motion (2.19) and (2.20) together with the vanishing of the two-dimensional divergence of the perturbed velocity,

$$\frac{\partial u}{\partial \xi} + i\beta v = 0, \tag{4.3}$$

yield Laplace's equation,

$$\frac{\partial^2 u}{\partial \xi^2} - \beta^2 u = 0, \tag{4.4}$$

for u. This result also follows upon setting $n = -1/2$ in equation (2.45). The dynamics are contained in the free-boundary condition (2.40) which, expressed in terms of u, reads

$$\sigma^2 \frac{\partial u}{\partial \xi} + [(2-q)\beta\sigma - g_{\rm eff}\beta^2]u = 0. \tag{4.5}$$

We insert the general solution

$$u = C \cosh \beta\xi + S \sinh \beta\xi, \tag{4.6}$$

into the boundary condition and arrive at

$$\begin{aligned} &\pm \sinh \beta\{\nu^2 \pm [(2-q) \coth \beta + 2q\beta]\nu + [q^2\beta^2 - (q^2+p^2-3)\beta \coth \beta]\}C \\ &+ \cosh \beta\{\nu^2 \pm [(2-q) \tanh \beta + 2q\beta]\nu + [q^2\beta^2 - (q^2+p^2-3)\beta \tanh \beta]\}S = 0, \end{aligned} \tag{4.7}$$

where the upper and lower signs refer to the boundaries at $\xi = \pm 1$.

The dispersion relation which follows from equation (4.7) is a quadratic equation in ν^2,

$$a\nu^4 + b\nu^2 + c = 0, \tag{4.8}$$

with

$$\begin{aligned} a &= 1, \\ b &= -\{(2-q)^2 + 2q^2\beta^2 + 2[(q-1)(3-q) + p^2]\beta \coth 2\beta\}, \\ c &= \beta^2\{(q^2+p^2-3)^2 + q^4\beta^2 - 2q^2(q^2+p^2-3)\beta \coth 2\beta\}. \end{aligned} \tag{4.9}$$

Next we establish that $c<0$ is a necessary and sufficient condition for the existence of an unstable mode if $3/2<q<2$. We begin by proving that the discriminant, $\Delta=b^2-4ac$, is positive for all β when q is in the specified range. This is accomplished by replacing coth β by 1 in the expressions for b and c thereby obtaining a lower limit for b^2 and an upper limit for c. These are combined to yield a lower limit for Δ. By grouping terms according to powers of β and p, it is straightforward to demonstrate that Δ is positive. Since $\Delta>0$, $a=1$, and $b<0$, all modes are stable for $c>0$. For $c<0$, there is a single growing mode which has a decaying complex conjugate partner. Their frequencies satisfy

$$\nu_-^2=\frac{-b-\sqrt{b^2-4ac}}{2a}. \tag{4.10}$$

To exhibit the parameter range within which the unstable mode exists, we rewrite c in the form

$$c=\beta^2q^4(\beta\tanh\beta-\beta_*)(\beta\coth\beta-\beta_*), \tag{4.11}$$

where

$$\beta_*=\frac{q^2+p^2-3}{q^2}. \tag{4.12}$$

The instability strip in the $\beta\beta_*$ plane has two regimes:

$p^2<3$, for which

$$\begin{aligned} &c<0 \quad \text{for} \quad \beta\tanh\beta<\beta_*,\\ &c>0 \quad \text{for} \quad \beta\tanh\beta>\beta_* \end{aligned} \tag{4.13}$$

and $p^2>3$, for which

$$\begin{aligned} &c>0 \quad \text{for} \quad \beta\coth\beta<\beta_*,\\ &c<0 \quad \text{for} \quad \beta\tanh\beta<\beta_*<\beta\coth\beta,\\ &c>0 \quad \text{for} \quad \beta\tanh\beta>\beta_*, \end{aligned} \tag{4.14}$$

The instability strip is drawn in Fig. 4(a). It follows from equations (4.7), (4.13) and (4.14) that on the right-hand boundary of the instability strip the eigenfunction is of the form $u=\cosh\beta\xi$, which is a buckling mode, whereas on the left-hand boundary above $\beta_*=1$ it is of the form $u=\sinh\beta\xi$, which is a sausage mode. Although the shape of the instability strip depends on q and p only through the combination β_*, the growth rate $Im\,\nu$, and the phase rotation of the eigenfunction across the ribbon, $Arg[(C\cosh\beta+S\sinh\beta)/(C\cosh\beta-S\sinh\beta)]$, vary with q at fixed β_*. Contour plots of these quantities are displayed in Fig. 4 (b) & (c) for the representative value of $q=1.85$.

The instability strip appropriate to the narrow torus with $N=0$ is confined to $0\leq\beta_*\leq0.25$, corresponding to $p=0$ and $\sqrt{3}\leq q\leq2$. This is clearly related to the discovery by PPII confirmed in Section 3 that the unstable low-β modes of narrow tori are restricted to $q>\sqrt{3}$ for arbitrary N.

4.2 EDGE WAVES

The gravitational and inertial forces enter the dynamics of the perturbed ribbon solely through the boundary condition, equation (4.5). Furthermore, it is obvious from equation (4.4) that the ribbon does not support internal waves. These are hints that the ribbon's unstable modes are related to waves which propagate along its boundaries. The study of edge waves in the narrow

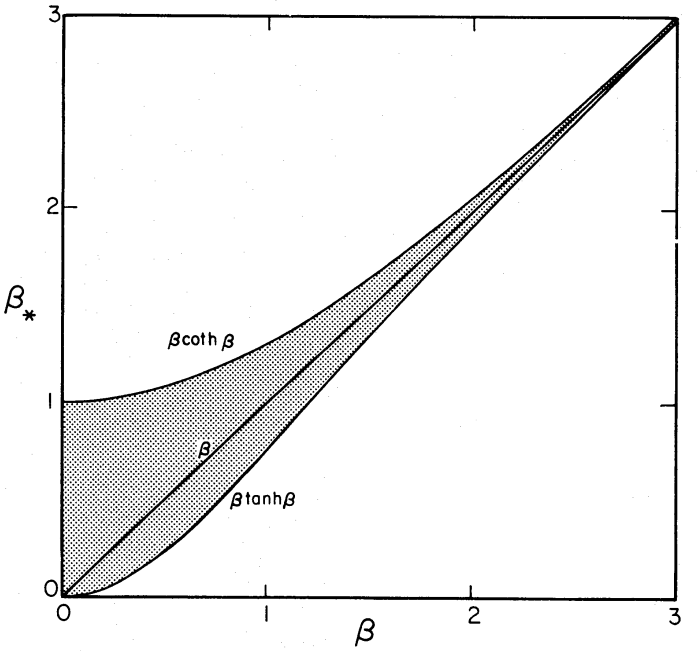

Figure 4. (a) Instability strip (shaded) in the $\beta\beta_*$ plane for coupled edge modes of the thin ribbon. The exponentially narrow region at the upper right requires a large inward gravity at the edges. The phase velocity of the upstream mode on an isolated edge vanishes along the line $\beta=\beta_*$.

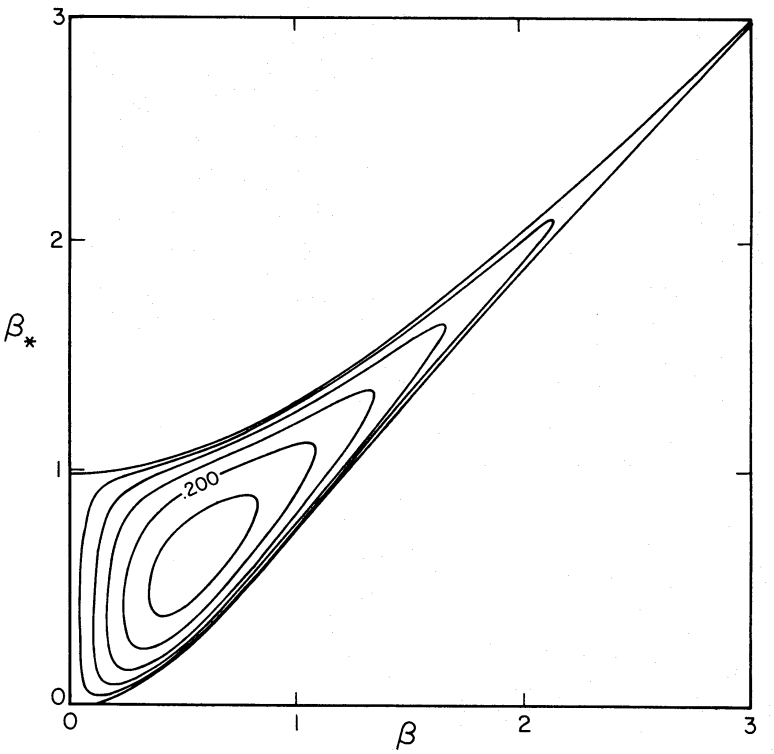

Figure 4. (b) The growth rate in units of the orbital frequency, $Im(\omega)/\Omega$, for the thin ribbon with $q=1.85$ and variable gravity parameter p.

ribbon is complicated by the interaction between the waves from opposition boundaries, at least for $\beta\leq 1$. To isolate an edge wave we remove the lower boundary from $\xi=-1$ to $\xi=-\infty$. The eigenfunction now takes the form

$$u=\exp(\beta\xi), \tag{4.15}$$

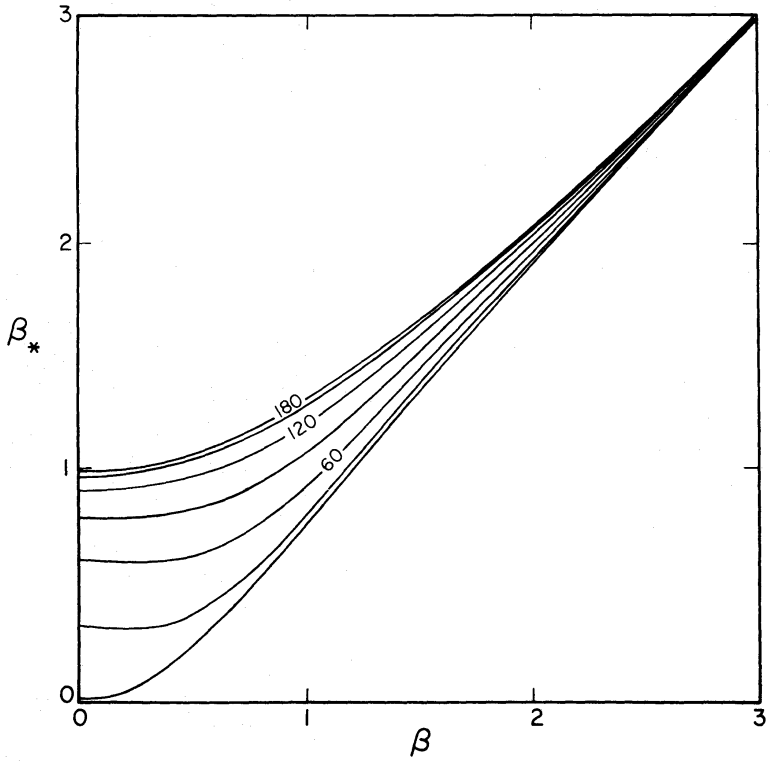

Figure 4. (c) Phase rotation in degrees of unstable modes of the thin ribbon for $q=1.85$ and variable p. The rotation is 0° for 'buckling' modes, 180° for 'sausage' modes.

and, when substituted into the boundary condition (4.5), yields the frequencies

$$\nu_{u,d}=-q\beta-\left(\frac{2-q}{2}\right)\pm\sqrt{\left(\frac{2-q}{2}\right)^2+(2q+p^2-3)\beta}. \tag{4.16}$$

The ν_u and ν_d frequencies are associated with stable edge waves which are convected by the fluid at the edge velocity $-q$ and propagate upstream and downstream, respectively. In the limit of vanishing rotation and vanishing shear, $p\to\infty$ and $q\to 0$, equation (4.16) reduces to $\nu=\pm p\sqrt{\beta}$, or in dimensional notation to $\omega=\pm\sqrt{gk}$, which is the dispersion relation for deep water waves.

The upstream propagating (slow) wave is of particular interest. Its phase velocity increases monotonically with increasing wavelength, from $-q$ at $\beta^{-1}=0$ to $(q^2+p^2-3)/(2-q)$ as $\beta^{-1}\to\infty$. For $\beta_\bullet>0$, the band of waves with $0<\beta\leq\beta_\bullet$ has positive phase velocity. Nearly stationary edge waves are important because matched pairs from opposite sides of the ribbon couple together to form pairs of zero-phase velocity modes. Since there is no corotation resonance, each pair consists of a growing and a decaying member which are complex conjugates of each other. In this context, we note that, for $p=0$, stationary edge waves exist for $q>\sqrt{3}$, the same condition required for the existence of unstable modes of the narrow torus.

4.3 UNSTABLE MODES AS COUPLED EDGE WAVES

To examine the relation between edge waves and unstable modes, we look first at an example for which the interaction between the waves from opposite sides of the ribbon is sufficiently weak so that the characteristics of the individual waves that comprise the mode are recognizable.

The most transparent example involves short ($\beta\gg 1$) waves since their coupling is exponentially small. Equation (4.16) shows that short ($\beta\gg 1$), stationary ($\beta=\beta_\bullet$), edge waves require $p\gg 1$; this is the motivation for the addition of the p^2 term to $g_{\rm eff}$. From equation (4.14) we deduce that for

$\beta_* \gg 1$ there is a narrow band of weakly unstable modes centred at $\beta=\beta_*$. The full width of the instability strip is

$$\Delta\beta = 4\beta_* \exp(-\beta_*), \tag{4.17}$$

and the maximum value of the growth rate is

$$Im\, \nu_* = q\beta_* \exp(-2\beta_*). \tag{4.18}$$

The short waves which couple together to form the unstable mode are closely related to deep water waves.

Another example, more relevant to the torus, involves long ($\beta \ll 1$) waves and $p^2<3$. The strong interaction between waves from opposite sides of the ribbon is reflected in the width of the band of unstable modes which stretches from $\beta=0$ to where $\beta \tanh \beta=\beta_*$.

Perhaps the most convincing piece of evidence for the identification of the unstable modes as coupled edge waves is Fig. 4(a) which shows the locus of the stationary edge waves, given by $\beta_*=\beta$, running through the middle of the instability strip. The figure also emphasizes that the two examples described above correspond to opposite ends of the instability strip.

5 Incompressible, constant-angular-momentum torus

As we noted earlier, PPI claimed to prove from a variational principle that the (three-dimensionally) incompressible, constant-angular-momentum torus ($n=0$, $q=2$) is stable; however, we pointed out that they did not use the appropriate, free-boundary condition, equation (2.29) in their argument. The matter is actually quite subtle. Their derivation of the variation principle was presented for finite compressibility, and only at the end did they consider the limit in which the adiabatic index $\Gamma \to 0$. With the free-boundary condition this limit is singular and when it is taken with care the proof of stability does not carry through. In this section, we demonstrate the instability of the case $q=2$ and $n=0$ by explicitly constructing the three-dimensional modes.

The vorticity, $\nabla \times \mathbf{V}$, vanishes in the equilibrium for $q=2$. Therefore by Kelvin's theorem (Landau & Lifshitz 1959), it may be assumed to vanish in perturbation as well. Hence the perturbed velocity can be written as

$$\mathbf{v}' = \nabla\psi, \tag{5.1}$$

and since the fluid is incompressible,

$$\nabla^2\psi = \nabla \cdot \mathbf{v}' = 0. \tag{5.2}$$

By comparing the z-component of equation (5.1) with the vertical equation of motion, equation (2.25), we see that

$$Q = i\sigma\psi. \tag{5.3}$$

Hence the free-boundary condition, equation (2.29) can be written

$$g_{\rm eff}\frac{\partial\psi}{\partial n} = \sigma^2\psi, \tag{5.4}$$

where $\partial/\partial n$ denotes the outward normal derivative at the surface, and $g_{\rm eff}$ is the effective gravity there (defined to be positive for inward acceleration).

Up to this point, the narrow-torus approximation has not been used in this section. We now make that simplification. By equation (2.13), the torus is circular in cross-section, and it is convenient to adopt cylindrical polar coordinates with the axis along the *azimuthal* direction:

$$x=\varrho\cos\theta, \qquad y=y, \qquad z=\varrho\sin\theta; \tag{5.5}$$

the radial coordinate ϱ runs from 0 at the pressure maximum to a at the surface of the torus and is not to be confused with the density of the fluid; since the latter is constant, it does not enter the equations of this section. In these coordinates, equation (5.2) becomes

$$\frac{1}{\varrho}\frac{\partial}{\partial\varrho}\left(\varrho\frac{\partial\psi}{\partial\varrho}\right)+\frac{1}{\varrho^2}\frac{\partial^2\psi}{\partial\theta^2}-k^2\psi=0, \tag{5.6}$$

and has the general solution

$$\psi(\varrho,\theta,y,t)=\exp(iky-i\omega t)\sum_{j=-\infty}^{\infty}C_j\exp(ij\theta)I_j(k\varrho) \tag{5.7}$$

for arbitrary complex constants $\{C_j\}$. Here $I_j(z)$ is the modified Bessel function of order j which is regular at the origin and converges throughout the complex plane (*cf.* Abramowitz & Stegun 1965). We note that $I_j(\beta)=I_{-j}(\beta)$. On the boundary, $\varrho=a$, $g_{\rm eff}=\Omega^2 a$, and $\sigma=\omega+2\beta\Omega\cos\theta\equiv 2\beta\Omega(\cos\theta-s)$. Putting these and equations (5.7) into equation (5.4) yields

$$[(s^2+\tfrac{1}{2})I_j(\beta)-I_j'(\beta)/4\beta]C_j-sI_{j-1}(\beta)C_{j-1}-sI_{j+1}(\beta)C_{j+1}+\tfrac{1}{4}I_{j-2}(\beta)C_{j-2}+\tfrac{1}{4}I_{j+2}(\beta)C_{j+2}=0,$$

$$j=0,\ \pm1,\ \pm2,\ \pm3,\ \ldots, \tag{5.8}$$

where $I_j'(\beta)\equiv dI_j(\beta)/d\beta$.

In order that the series given by equation (5.7) converge, the boundary condition,

$$I_j(\beta)C_j\to 0 \quad \text{as} \quad j\to\pm\infty, \tag{5.9}$$

must be satisfied. We shall see in a moment that the recursion relation (5.8) has four linearly independent asymptotic behaviours for $j\to\pm\infty$ and that only two of these behaviours satisfy equation (5.9). The permissible asymptotic solutions near $j=-\infty$ connect *via* equation (5.8) to permissible solutions near $j=+\infty$ only if s takes on discrete values depending on β. Thus equations (5.8) and (5.9) together constitute a linear eigenvalue problem. The modified Bessel function $I_j(z)$ can be represented by the power series

$$I_j(z)=\left(\frac{z}{2}\right)^{|j|}\sum_{k=0}^{\infty}\frac{(z^2/4)^k}{k!(k+|j|)!}. \tag{5.10}$$

Thus

$$I_j(\beta)\to\frac{1}{j!}\left(\frac{\beta}{2}\right)^j \quad \textit{as} \quad j/\beta^2\to\infty, \tag{5.11}$$

so that equation (5.8) asymptotically simplifies to

$$[(s^2+\tfrac{1}{2})-j/4\beta^2]C_j-\frac{2j}{\beta}sC_{j-1}-\frac{\beta}{2(j+1)}sC_{j+1}+\frac{j(j-1)}{\beta^2}C_{j-2}+\frac{\beta^2}{16(j+1)(j+2)}C_{j+2}=0. \tag{5.12}$$

There are two possible dominant balances (*cf.* Bender & Orszag 1978):

$$C_j\approx 4jC_{j-2},$$

$$\frac{I_j(\beta)C_j}{I_{j-2}C_{j-2}}\approx\frac{\beta^2}{j} \quad \text{as} \quad j\to\infty; \tag{5.13a}$$

or

$$C_j\approx\frac{\beta^4}{4j^3}C_{j+2},$$

$$\frac{I_j(\beta)C_j}{I_{j-2}C_{j-2}}\approx\frac{j}{\beta^2} \quad \text{as} \quad j\to\infty. \tag{5.13b}$$

It can be verified in each case that the neglected terms of equation (5.12) are small compared to those in the dominant balance if

$$C_j/C_{j-1} \propto \sqrt{C_j/C_{j-2}}. \tag{5.14}$$

Clearly equation (5.13a) meets the convergence criterion given by equation (5.9) but equation (5.13b) does not. Similar reasoning applies for $j \to -\infty$. Because even and odd values of j are asymptotically decoupled by both balances,★, equations (5.13a) and (5.13b) together make four linearly independent asymptotic solutions of equation (5.8).

Since the forms of equations (5.8) and (5.9) are unchanged by the replacement $j \to -j$, one can demand that $C_j = \pm C_{-j}$ – that is, solutions should be either symmetric or anti-symmetric. These correspond respectively to $\psi(x, y, -z, t) = \pm\psi(x, y, z, t)$.

We have solved equations (5.8)–(5.9) for general β by Newton–Raphson iteration. An integer $L \gg \beta^2$ is chosen and C_L is set to 1. At the start of each iteration, we have estimates for the two parameters s and $f \equiv C_{L+1}/C_L$; C_{L+2} and C_{L+3} are then calculated from equation (5.13a). The recursion relation (5.8) is used to compute $C_{L-1,\ldots}, C_{-1}, C_{-2}$. If we seek a symmetric solution, the errors at this stage are

$\varepsilon_1 = C_{-1} - C_1$,

$\varepsilon_2 = C_{-2} - C_2$;

otherwise, for antisymmetric solutions,

$\varepsilon_1 = C_0$,

$\varepsilon_2 = C_{-1} + C_1$.

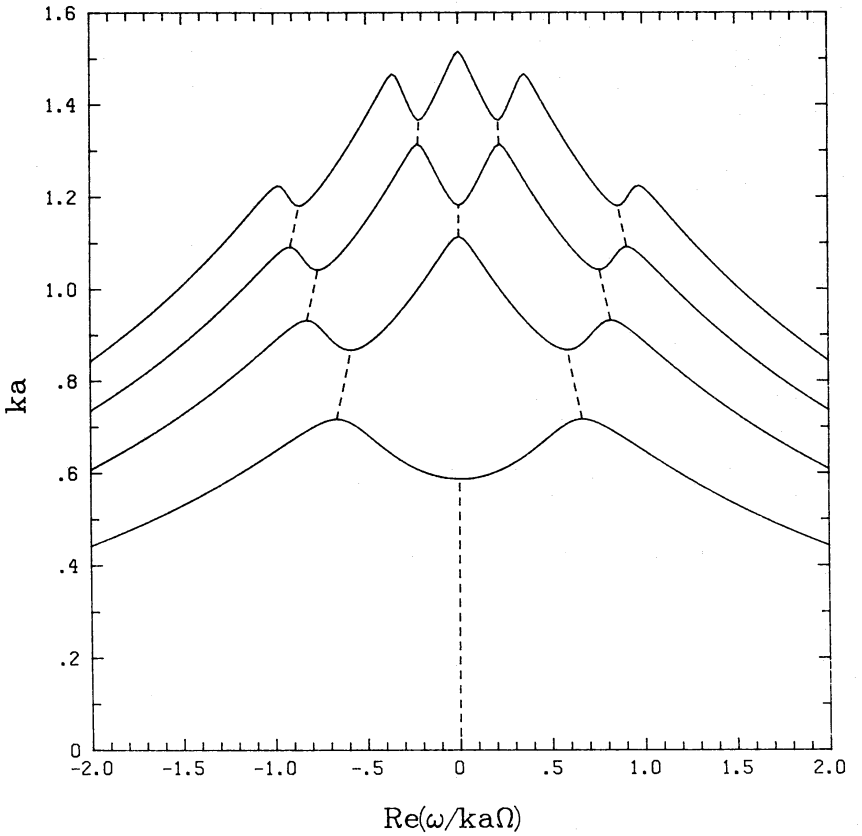

Figure 5. (a) The real part of the dispersion relation for the incompressible, constant-angular-momentum torus, $n=0$, $q=2$. The unstable modes are indicated by dashed lines and have corotation within the torus, $|\mathrm{Re}(\omega/ka\Omega)|<2$.

★ that is, an arbitrary constant of proportionality occurs in equation (5.14).

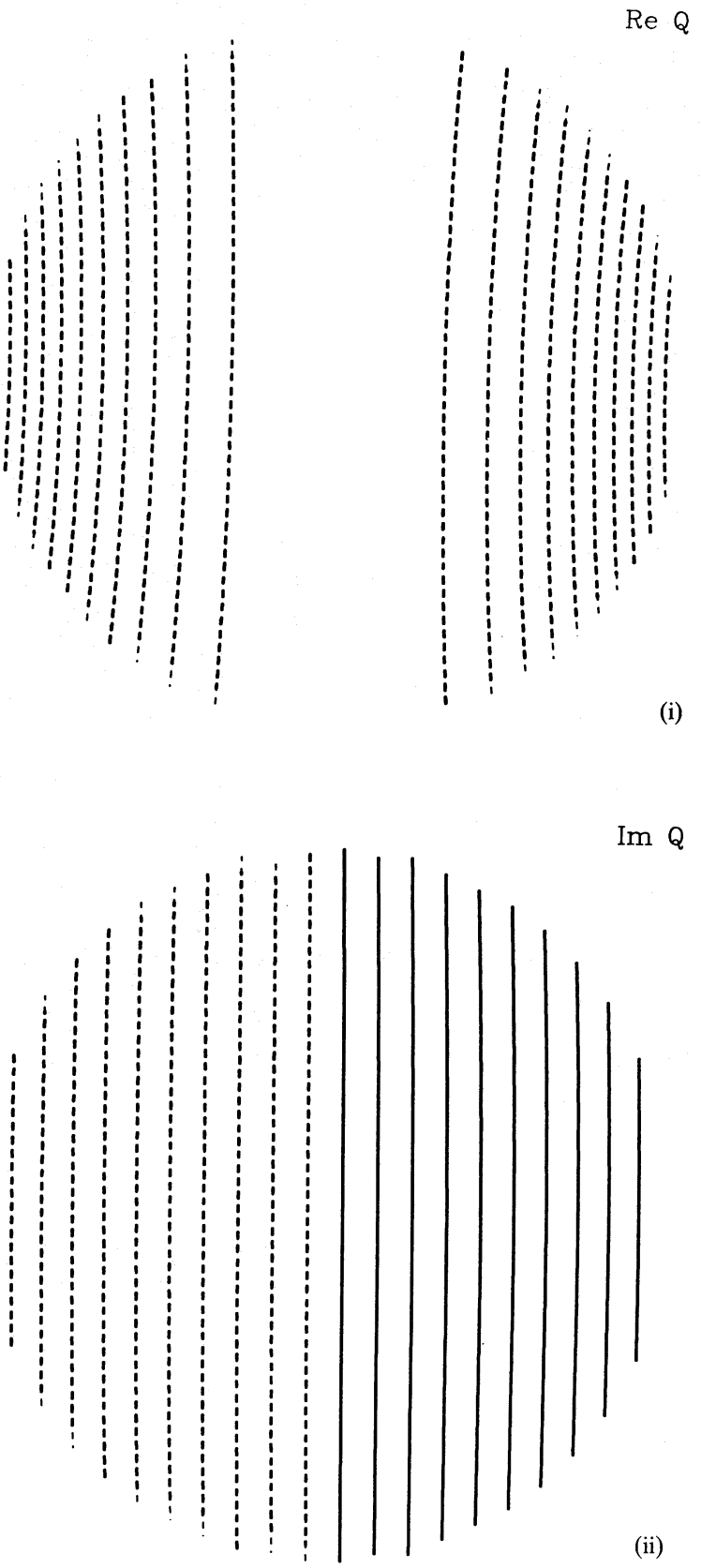

Figure 5. (b) Contours in the meridional plane of the perturbed enthalpy for the fastest growing mode (β=0.38, ω=0.287Ωi) of the incompressible, constant-angular-momentum torus. Positive and negative values correspond to solid and dashed contours. (i) Re(Q), (ii) Im(Q).

By making small changes in s and f, we estimate the first partial derivatives of $(\varepsilon_1, \varepsilon_2)$ with respect to (s, f) and obtain improved estimates for s and f in the standard way. When this process converges, it does so quickly. An important detail is that for symmetric modes having $Re(s)=0$, either all of the odd- or all of the even-indexed C_j vanish, whence $f\to 0$ or $f\to\infty$ according to the parity of L. It is important for the convergence of the iteration to choose this parity so that $f\to 0$.

Fig. 5(a) shows the real part of the dispersion relation obtained by this numerical procedure for the symmetric modes. The principal unstable branch extends from $\beta=0$ to $\beta_c\approx 0.587$; for comparison, the height-averaged equations (2.38)–(2.40) for $q=2$ and $n=0$ predict $\beta_c\approx 0.596$. The maximum growth rate in units of Ω is 0.287, as compared to 0.288 from (2.38)–(2.40), and occurs at $\beta_{max}\approx 0.38$ in both cases. Fig. 5 (b) (i) & (ii) are contour plots of the real and imaginary parts of Q in the meridional xz planes for the fastest-growing mode. Note the approximate constancy of Q with height.

Evidently the height-averaged equations make very accurate predictions for the principal branch. Furthermore, the errors are likely to be even smaller for any $n>0$ or $q\in[\sqrt{3}, 2)$. In the limit $n\to\infty$ (an isothermal thin torus) and $q=2$, PPI have shown that the three-dimensional equation (2.27) separates in the coordinates (x, y, z) and that the unstable modes are exactly constant along z;★ their argument can easily be generalized to $q\neq 2$. Thus the error committed by height averaging vanishes in the limit $n\to\infty$, and while it is not proven that the error decreases monotonically with increasing n, the perturbative analysis of the Appendix supports this conjecture. As regards the variation with q, we note that β_c decreases with q and vanishes as $q\to\sqrt{3}$. Since vertical hydrostatic equilibrium holds for small β, we may expect the errors on the principal branch to decrease with q also.

Fig. 5(a) indicates that there are higher branches of instability at values of β above those on the principal branch. These branches and their generalization to other values of n and q will form the subject of a later paper. They are not well represented, except in certain qualitative features, by height-averaged equations. They have somewhat lower growth rates than the modes of the principal branch, but their instability persists to $q<\sqrt{3}$. For an extended disc, all growth rates tend to zero as $q\to 3/2$, except possibly for modes having corotations close to a sharp inner or outer edge of the disc, should such exist.

When $\beta\ll 1$, power-series solutions to equations (5.8)–(5.9) can be determined analytically. We shall derive here only the lowest order non-trivial terms. As $\beta\to 0$, equation (5.11) implies that the coefficient of C_0 in equation (5.8) for $j=0$ must vanish, whence

$$s=\pm i\sqrt{\frac{3}{8}}+O(\beta^2). \tag{5.15}$$

It has been assumed implicitly here that the ratios C_j/C_0 do not blow up as $\beta\to 0$; by comparing equations (5.13a) and (5.13b) one sees that this assumption is equivalent to the correct boundary condition at $|j|/\beta^2=\infty$. Examining equation (5.9) for $j=1$ and $j=2$, we then find using equation (5.15) that

$$C_{-1}=C_{+1}=\mp\beta 4i\sqrt{\frac{3}{2}}+O(\beta^3),$$

$$C_{-2}=C_{+2}=4+O(\beta^3).$$

★ At $n=\infty$, the boundary of the torus occurs infinitely far from the pressure maximum in units of the density scale length c/Ω, where c is the sound speed; the free-boundary condition can then be replaced by the requirement that $Q\to 0$ at infinity; the latter condition is of course compatible with this separation of variables.

Therefore, the lowest order expression for the velocity potential is

$$\psi = I_0(k\varrho) \mp 8i\beta \sqrt{\frac{3}{2}}\, I_1(k\varrho) \cos\theta + 8I_2(k\varrho) \cos 2\theta + O(\beta^4)$$

$$= 1 \mp 4i \sqrt{\frac{3}{2}}\, \beta k x + \frac{k^2(5x^2 - 3z^2)}{4} + O(\beta^4). \tag{5.16}$$

6 Discussion

We have shown that the long-wavelength unstable modes of the two-dimensionally incompressible ribbon are coupled edge waves. As stressed in Section 3, the similarity between the long-wavelength modes of this system and those of tori with arbitrary q and n suggests by continuity that the same mechanism operates in these systems as well. Of course, in a compressible torus the edge modes propagate not along the physical edge of the torus but along the natural soft edge provided by the density gradient. The distinction between the edge modes and the truly sonic modes is more than semantic. For example, with $q<2$ sufficiently long-wavelength sound waves with corotation at the pressure maximum are non-propagating (i.e. evanescent) inside the torus, because the frequency in the frame comoving with the fluid, σ, is smaller than the epicycle frequency, $\varkappa$. For $N=0$, stationary waves on an isolated edge exist only for $q>\sqrt{3}$; this explains the restriction of the low-β unstable modes to $q>\sqrt{3}$ in this case. The fact that the same condition applies for all n (PPII) is another indication that the unstable modes are not sound waves.

The most unstable modes grow on the dynamical time-scale Ω^{-1} which suggests that they pose a serious problem to the survival of thick accretion tori. Because vertical hydrostatic equilibrium is such an excellent approximation for the low-β modes, two-dimensional hydrodynamical calculations may suffice to describe the non-linear evolution of unstable accretion tori.

The higher-β unstable modes, which exist even for $q<\sqrt{3}$, may be investigated by means of three-dimensional linear stability calculations. The surface character and slower growth rates of these modes imply that they may saturate at amplitudes sufficient to provide a significant 'viscosity' but not so large as to threaten the existence of the torus. Unfortunately, these traits will probably make the non-linear evolution of these modes extremely difficult to simulate.

Further work is also needed to extend the investigations reported here to wider tori which are of more relevance to astrophysics. It remains to be seen how well the results obtained for slender tori apply to their wider relations.

Acknowledgements

We thank Roger Blandford for encouragement and advice and John Papaloizou and Jim Pringle for sending us their papers far in advance of publication. We note that Omar Blaes and Wolfgang Glatzel have independently derived many of the results reported in this paper. Our research was supported in part by the NSF through grants AST83-13725 and AST82-13001.

References

Abramowitz, M. & Stegun, I. E., 1965. *Handbook of Mathematical Functions*, Dover, New York.

Begelman, M. C., Blandford, R. D. & Rees, M. J., 1984. *Rev. Mod. Phys.*, **56**, 255.

Bender, C. M. & Orszag, S. A., 1978. *Advanced Mathematical Methods For Scientists And Engineers*, McGraw-Hill, New York.

Blaes, O. M., 1985. Preprint.

Blandford, R. D. & Znajek, R. L., 1977. *Mon. Not. R. astr. Soc.*, **179**, 433.

Fishbone, L. G. & Moncrief, V., 1976. *Astrophys. J.*, **207**, 962.

Goldreich, P. & Narayan, R., 1985. *Mon. Not. R. astr. Soc.*, **213,** 7P.
Grinfield, M. A., 1984. *Geophys. Astrophys. Fluid Dynamics*, **28,** 31.
Jaroszyński, M., Abramowicz, M. A. & Paczyński, B., 1980. *Acta Astr.*, **30,** 1.
Kozłowski, M., Wiita, P. J. & Paczyński, B., 1979. *Acta Astr.*, **29,** 157.
Landau, L. D. & Lifshitz, E. M., 1959. *Fluid Mechanics*, Pergamon Press, Oxford.
Lynden-Bell, D., 1978. *Phys. Scripta*, **17,** 185.
Margon, B., 1984. *Ann. Rev. Astr. Astrophys.*, **22,** 507.
Paczyńsky, B. & Wiita, P. J., 1980. *Astr. Astrophys.*, **88,** 23.
Papaloizou, J. C. B. & Pringle, J. E., 1984. *Mon. Not. R. astr. Soc.*, **208,** 721, (PPI).
Papaloizou, J. C. B. & Pringle, J. E., 1985. *Mon. Not. R. astr. Soc.*, **213,** 799, (PPII).
Rayleigh, Lord, 1880. *Proc. London Math. Soc.*, **11,** 57.
Rayleigh, Lord, 1916. *Proc. R. Soc. London A*, **93,** 148.
Rees, M. J., 1980. In: *Extragalactic X-ray Astronomy*, p. 339, eds Giaconi, R. & Seti, G., Reidel, Dordrecht, Holland.
Rees, M. J., Begelman, M. C., Blandford, R. D. & Phinney, E. S., 1982. *Nature*, **295,** 17.
Rees, M. J., 1984. *Ann. Rev. Astr. Astrophys.*, **22,** 471.
Shakura, N. I. & Sunyaev, R. A., 1973. *Astr. Astrophys.*, **24,** 337.

Appendix

Here we sketch the procedure used to obtain the correction, Δs, due to vertical acceleration, to the hydrostatic eigenvalue, $s_{\rm HS}$, obtained from the height-integrated equation (2.38). Thus we write

$$s=s_{\rm HS}+\Delta s. \tag{A1}$$

From equation (2.33) we have

$$Q(x,\,z)=Q_{\rm HS}(x)+\Delta Q(x)+\delta Q(x,\,z), \tag{A2}$$

where

$$\delta Q(x,\,z)=\frac{(\Omega z)^2}{2}\,\Theta(x). \tag{A3}$$

Changing to dimensionless variables we obtain

$$\Theta(\xi)=\frac{\sigma^2}{D(1-\xi^2)}\left\{\xi\,\frac{dQ_{\rm HS}}{d\xi}+\left[\frac{D}{(2q-3)}-\frac{2\beta\xi}{\sigma}\right]Q_{\rm HS}\right\}, \tag{A4}$$

where we have used the symbols σ and D to denote the obvious dimensionless versions of the expressions defined in Section 2.2: $\sigma=q\beta(\xi-s)$, $\varkappa=2(2-q)$, and $D=\varkappa^2-\sigma^2$.

Next we derive an inhomogeneous version of equation (2.38) which accounts for the departure from strict hydrostatic equilibrium. We substitute equation (A2) into equation (2.27) and expand the terms which contain the eigenvalue, s, according to equation (A1). The resulting expression is then averaged over z and the contributions from δQ and Δs, which are evaluated with the hydrostatic eigenfunction, $Q_{\rm HS}$, are collected on the right-hand side of the equation (2.38) and treated as an inhomogeneous term. The inhomogeneous term consists of two pieces:

$$IHT_\Theta=-\frac{(2q-3)(1-\xi^2)}{2(2n+3)}\left\{\frac{d^2\Theta}{d\xi^2}-\left[\frac{(2n+3)\xi}{(1-\xi^2)}-\frac{2q\beta\sigma}{D}\right]\frac{d\Theta}{d\xi}\right.$$
$$\left.-\left[\frac{(2n+3)D}{(2q-3)(1-\xi^2)}-\frac{2(2n+3)\beta\xi}{\sigma(1-\xi^2)}+\frac{4q\beta^2}{D}+\beta^2\right]\Theta\right\}, \tag{A5}$$

and

$$IHT_{\Delta s}=\Delta s\left\{\left[\frac{2(q\beta)^2}{D}+\frac{4(q\beta)^2\sigma^2}{D^2}\right]\frac{dQ_{\rm HS}}{d\xi}\right.$$
$$\left.+\left[\frac{2(2n+1)q\beta\sigma}{(2q-3)(1-\xi^2)}-\frac{2(2n+1)q\beta^2\xi}{\sigma^2(1-\xi^2)}-\frac{8q^2\beta^3\sigma}{D^2}\right]Q_{\rm HS}\right\}. \quad \text{(A6)}$$

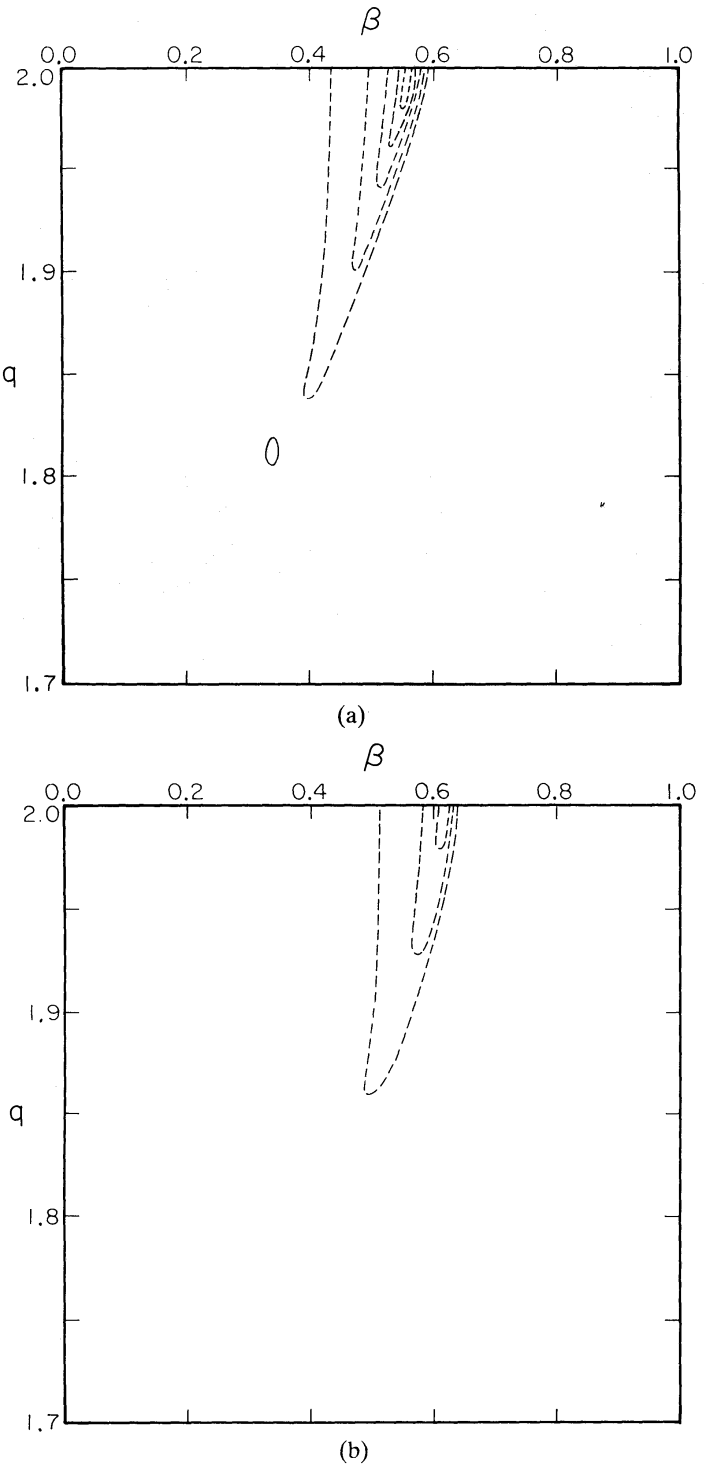

Figure A1. Contour plots of the correction Δs to the scaled growth rate $Im(\omega)/(-q\beta\Omega)$ due to departures from vertical hydrostatic equilibrium, for (a) $n=0$, (b) $n=1/2$. Positive and negative values correspond to solid and dashed contours. Lowest contour levels at ± 0.002. Contour separation 0.004.

If we denote the second-order linear differential operator in equation (2.38) by $\mathscr{L}_2$ then

$$\mathscr{L}_2(\Delta Q)=IHT\equiv IHT_\Theta+IHT_{\Delta s}. \tag{A7}$$

We are already familiar with $Q_{\rm HS}$, the homogeneous solution of equation (A7) which is regular at the boundaries, $\xi=\pm1$. We denote by $Q'_{\rm HS}$ the other homogeneous solution, which is irregular at the boundaries. The general solution of equation (A7) may be expressed in terms of the homogeneous solutions as

$$\Delta Q(\xi)=\int_{-1}^{\xi} d\eta\left[\frac{Q_{\rm HS}(\xi)Q'_{\rm HS}(\eta)-Q'_{\rm HS}(\xi)Q_{\rm HS}(\eta)}{W(\eta)}\right]IHT(\eta), \tag{A8}$$

where the wronskian W is given by

$$W(\xi)\propto\frac{D(\xi)}{(1-\xi^2)^{(n+\frac{1}{2})}}. \tag{A9}$$

The requirement that $\Delta Q(\xi)$ satisfy the same boundary conditions (2.40) as the regular homogeneous solution, $Q_{\rm HS}(\xi)$, implies

$$\int_{-1}^{+1} d\xi\,\frac{IHT(\xi)Q_{\rm HS}(\xi)}{W(\xi)}=0. \tag{A10}$$

The value of Δs is obtained from numerical integration of equation (A10) using $Q_{\rm HS}$ obtained from equation (2.38). Fig. A1(a & b) display contour plots of the correction to the eigenvalue for $n=0$ and $n=1/2$ and show that the hydrostatic approximation is astonishingly good. At maximum growth rate $|\Delta s|<0.01|s_{\rm HS}|$. The larger corrections, which occur near the upper boundary ($\beta\to\beta_c$) of the unstable zone, occur because there is a small non-hydrostatic correction to the location of the boundary and $Im(\omega/\Omega)$ declines steeply to zero as $\beta\to\beta_c$.